ACS APPLIED MATERIALS & INTERFACES

Research Article

Cite This: ACS Appl. Mater. Interfaces 2017, 9, 44938−44947

www.acsami.org

# Spontaneous Periodic Delamination of Thin Films To Form Crack-Free Metal and Silicon Ribbons with High Stretchability

Qiuting Zhang,[†] Yichao Tang,[†] Maryam Hajfathalian,[‡] Chunxu Chen,[§] Kevin T. Turner,[§] Dmitriy A. Dikin,[‡] Gaojian Lin,[†] and Jie Yin*[,†]

[†]Applied Mechanics of Materials Laboratory, Department of Mechanical Engineering, Temple University, 1947 North 12th Street, Philadelphia, Pennsylvania 19122, United States

[‡]Department of Mechanical Engineering, Temple University, 1947 North 12th Street, Philadelphia, Pennsylvania 19122, United States

[§]Department of Mechanical Engineering and Applied Mechanics, University of Pennsylvania, Philadelphia, Pennsylvania 19104, United States

Supporting Information



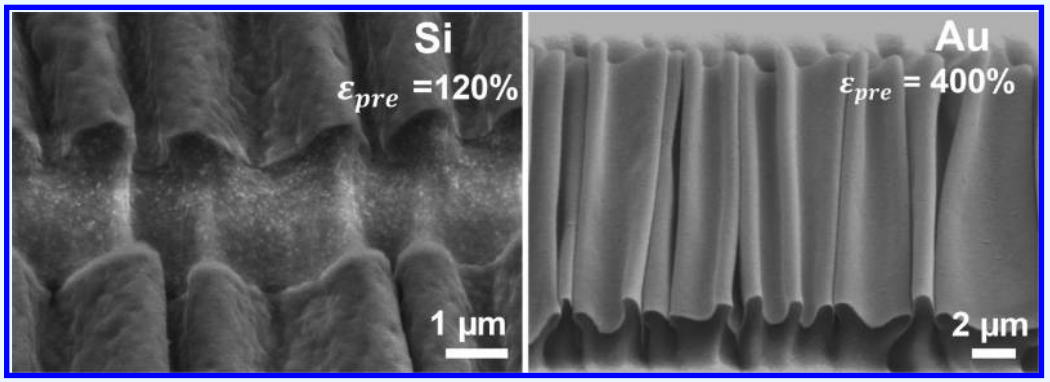


**ABSTRACT:** Design of electronic materials with high stretchability is of great importance for realizing soft and conformal electronics. One strategy of realizing stretchable metals and semiconductors is to exploit the buckling of materials bonded to elastomers. However, the level of stretchability is often limited by the cracking and fragmentation of the materials that occurs when constrained buckling occurs while bonded to the substrate. Here, we exploit a failure mechanism, spontaneous buckling-driven periodic delamination, to achieve high stretchability in metal and silicon films that are deposited on prestrained elastomer substrates. We find that both globally periodic buckle-delaminated pattern and ordered cracking patterns over large areas are observed in the spontaneously buckle-delaminated thin films. The geometry of periodic delaminated buckles and cracking periodicity can be predicted by theoretical models. By patterning the films into ribbons with widths smaller than the predicted cracking periodicity, we demonstrate the design of crack-free and spontaneous delaminated ribbons on highly prestrained elastomer substrates, which provides a high stretchability of about 120% and 400% in Si and Au ribbons, respectively. We find that the high stretchability is mainly attributed to the largely relaxed strain in the ribbons via spontaneous buckling-driven delamination, as made evident by the small maximum tensile strain in both ribbons, which is measured to be over 100 times smaller than that of the substrate prestrain.

**KEYWORDS:** *crack-free ribbons, extreme stretchability, spontaneous periodic buckle-delamination, metal and silicon thin films, crack fragmentation*

## INTRODUCTION

Harnessing buckling instabilities of materials and structures at small scales, such as buckling, wrinkling, creasing, folding, and delamination, has received tremendous interest due to their broad set of potential applications,[1−10] including surface-related tunable wetting, adhesion, friction, and optical properties, as well as structure-related functionalities in bistable switches in micro-electromechanical systems (MEMS),[11,12] stretchable electronics and devices,[13−16] and self-assembly fabrication of 3D mesostructures.[17,18] Despite the promise, challenges and limitations remain in harnessing compression-induced buckling instabilities.

First, unlike extensively studied wrinkling without debonding, harnessing the benefits of spontaneous buckling-driven delamination has received much less attention[19,20] and has been hindered by its localization characteristics,[21−27] which is in

Received: October 16, 2017
Accepted: November 28, 2017
Published: November 28, 2017




DOI: 10.1021/acsami.7b15693
ACS Appl. Mater. Interfaces 2017, 9, 44938−44947

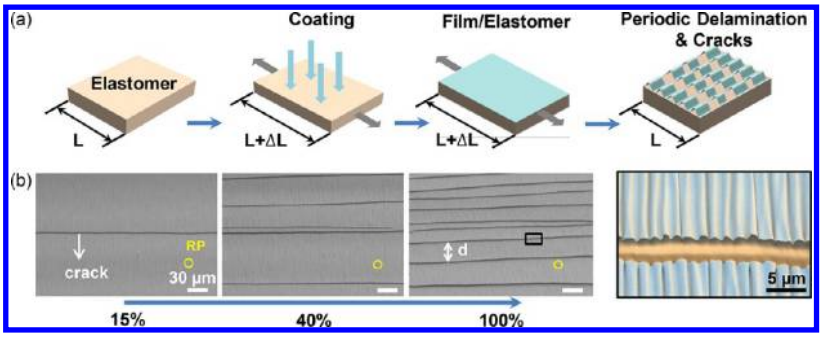


**Figure 1.** Global ordered buckle-delaminated and cracking pattern in thin films during their spontaneously buckling-driven delamination on largely prestrained elastomers. (a) Schematic illustration of generating spontaneous buckled delamination of thin films on prestrain elastomers. (b) SEM images of evolution of periodic crack formation in buckled delaminated Au thin films ($t$ = 40 nm) on a 100% prestrained PDMS substrate with the release of prestrain. Right side shows the magnified view of the delaminated buckles at a crack.

sharp contrast to its counterpart wrinkling with global and periodic patterns over large areas. Compared to wrinkling, one of the advantages of buckle-delamination is that the strain energy in the system can potentially be far more effectively released through both buckling and delamination, thus enabling a potential higher level of stretchability.[19,20,28] The potential of buckling-driven delamination as a method for achieving large stretchability in stretchable electronics was first articulated by Sun et al., in their work of controllable delamination of semiconductor ribbons.[29] They showed that, compared to spontaneous buckling without debonding,[30] controllable buckling-driven delamination by prepatterning adhesion spots on the substrate can more effectively release the strain in the semiconductor ribbons, thus providing approximately 3 times more stretchability. However, there are limited studies on controllable spontaneous buckle-delamination without prepatterned adhesion sites on substrates.[19,20] Second, another challenge of harnessing compressive buckling instability lies in the cracking. During buckling of a thin film on substrates with or without delamination, film cracking is often observed in a direction aligned normal to delaminated buckles[20] or wrinkles[31] because of the Poisson deformation of the substrate. The cracking failure can significantly degrade both mechanical and electrical performance and limit the ability to reach high stretchability. However, the study of crack formation and crack prevention during buckling-driven delamination remains largely unexplored.[19,20,29,32]

Here, we exploit the generation of controllable, globally periodic delaminated buckling patterns in thin films and microribbons made of metal and silicon materials through spontaneous buckle-delamination on highly prestrained (>100%) elastomer substrates. We find that, upon release of the high prestrains, a large-area, highly ordered pattern of both periodic buckle-delamination and cracking is formed in the thin films. A systematic study on the quantitative mechanism of spontaneous periodic buckle-delamination and cracking is conducted and understood through a combination of experimental characterization, theoretical modeling, and finite element simulation. We develop a related theoretical mechanics model to predict the geometry of the periodic delaminated buckles, as well as the periodicity of the cracking pattern. To eliminate the cracks in buckle-delaminated thin films, we apply the crack space model to the design of crack-free buckle-delaminated ribbons by using it to set widths of patterned ribbons. Finally, we demonstrate the application of the mechanics models to realize crack-free buckled ribbons with high stretchability in silicon (~120%) and gold (~400%) by harnessing spontaneous buckling delamination.

## EXPERIMENTAL SECTION

**Elastomer Substrates.** PDMS Sylgard (R) 184 (Dow Corning Corporation) consists of two components, prepolymer and cross-linker (PDMS, polydimethylsiloxane). The PDMS substrates of 0.3 mm thickness were prepared by mixing prepolymer and cross-linker at 10:1 weight ratio in a Petri dish and curing at 60 °C for 4 h. Dog-bone-like shape slabs were cut from the cured piece and cleaned with isopropyl alcohol. A customized designed stretch holder printed by 3D printer was used to prestretch PDMS substrate to a specific degree of strain. The commercial silicone rubbers with 0.45 MPa Young's modulus were cut into the same dog-bone shape as PDMS substrate, and then, high prestretching strains up to 400% were applied before depositing the films.

**Film Deposition.** A model 681 Gatan high-resolution ion beam coater was used to deposit the thin gold and copper film (20−100 nm thick) on prestretched elastomeric substrates under a base pressure of $1 \times 10^{-6}$ Torr at room temperature. The beam energy was 6 keV with 200 $\mu$A Penning gun currents carrying out the film deposition. The gold deposition rate was 13 nm/min. A magnetron sputtering system (Explore 14, Denton Vacuum) was used to deposit silicon on PDMS substrate under a base pressure of $3 \times 10^{-7}$ Torr at room temperature. The gas pressure was controlled around 3.0 mTorr in the chamber during the deposition. The deposition rate of silicon was close to 6 nm/min.

**Fabrication of Microribbons.** Commercially available TEM grids, G300P−Ni or G400P−Ni, were used as a shadow mask. The shadow mask was placed directly on the prestretched PDMS substrates to generate the patterned ribbons. For G300P−Ni and G400P−Ni masks, the grid bar is 35 and 40 $\mu$m, and the gap between them is 48 and 22 $\mu$m, respectively. A magnet placed underneath the PDMS was used to tightly bond these Ni grids to the PDMS substrate. After thin films of different materials were deposited, the masks were removed using the deionized water. It should be noted that, despite the simplicity of using a shadow mask in creating the ribbon pattern on the PDMS substrate, it remains challenging for a scale-up production, and other cost-effective patterning methods including transfer printing and substrate treatment[33−36] will be possible for ribbon fabrication.

**Surface Topography Characterization.** An SEM Quanta FEG 450 (FEI Co.) scanning electron microscope was used to characterize the surface morphology of thin film and ribbons. The low-vacuum chamber mode was selected because of the nonconductivity of PDMS. Samples were tilted 45° to observe the buckled wavy structures. Atomic force microscopy (AFM) was used to characterize the profile of wavy ribbons evolution during the releasing process.

**Finite Element Method (FEM) Simulation.** The Au thin film is modeled as an isotropic, linear elastic material with Young's modulus of 61 GPa and Poisson's ratio of 0.35.[37] The PDMS substrate is modeled as a hyperelastic neo-Hookean material with Young's


DOI: 10.1021/acsami.7b15693
ACS Appl. Mater. Interfaces 2017, 9, 44938−44947

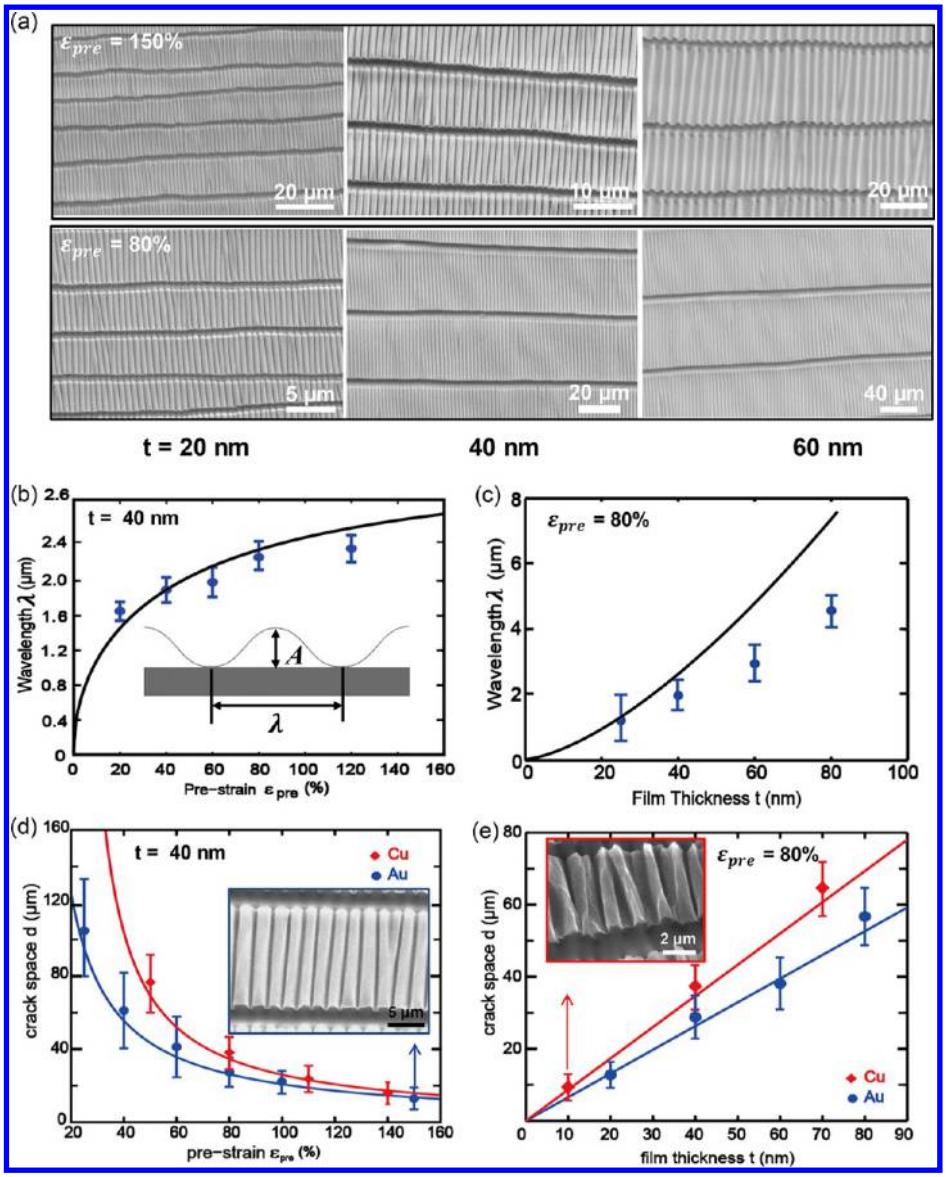


**Figure 2.** Prediction of the buckle-delaminated geometry and the average width of cracked fragments, i.e., crack space *d*, in spontaneous buckling-driven delamination of Au and Cu thin films on prestrained PDMS elastomers. (a) SEM images of cracking patterns in spontaneous buckling delamination of Au film with thickness ranging from 20 to 60 nm on prestrained PDMS substrate with $\varepsilon_{pre}$ = 150% (top row) and 80% (bottom row). Tilt view angle = 45° for all the SEM images. Comparison of delamination wavelength $\lambda$ in Au films on PDMS substrate between theory and experiments as a function of (b) substrate prestrain $\varepsilon_{pre}$ and (c) film thickness *t*. Comparison between the theoretical model (solid curves) and experimental measurements (symbols) on *d* in Au and Cu thin films as a function of (d) substrate prestrain $\varepsilon_{pre}$ and (e) film thickness *t*. Insets are the magnified view of the SEM of delaminated Au (*t* = 40 nm, $\varepsilon_{pre}$ = 150%) in part d and Cu films (*t* = 10 nm, $\varepsilon_{pre}$ = 80%) in part e on PDMS.

modulus of 2 MPa and Poisson's ratio of 0.49. Cohesive elements are added between the thin film and substrate to model the interfacial delamination behavior with linear elastic traction separation laws. The interfacial toughness between Au film and PDMS substrate is initially set as $\Gamma$ = 3 J/m$^2$ (see ref 38) to simulate the spontaneous delamination process. An increased value of $\Gamma$ is used to simulate the transition to wrinkling without debonding.

**Resistance Test.** First, 10 Au ribbons of 80 nm thickness were deposited on the top of 200% prestretched silicone rubber substrates. Each Au ribbon is 60 $\mu$m in width and 5 mm in length. Silver paste and fine wires were used to connect ribbons at both ends after they were fully relaxed. Samples are restretched step by step with a stretch holder to evaluate their electrical resistance change as a function of the applied strain. The cyclic strains are between 0% and 200% or 0% and 100% with a strain rate of 0.005/s.

## RESULTS AND DISCUSSION

**Both Spontaneously Periodic Buckle-Delaminated and Cracked Thin Films over Large Areas.** Figure 1a schematically illustrates the process for generating spontaneously buckling-driven periodic delaminated patterns by depositing a thin film on a prestretched (>100%) elastomer substrate. When the large substrate prestrain, $\varepsilon_{pre}$, is released, the film is placed in compression along the stretching direction, leading to a buckled film with periodic delamination. In the transverse direction, the film is placed in tension due to the Poisson expansion of the substrate, causing the cracking of the film into narrow strips.[20,31] As a demonstration, we deposited a gold thin film (Au, thickness *t* = 40 nm) on a prestretched polydimethylsiloxane (PDMS) substrate (thickness *h* = 0.3 mm) with $\varepsilon_{pre}$ = 100%. To evaluate the evolution and cracking


DOI: 10.1021/acsami.7b15693
ACS Appl. Mater. Interfaces 2017, 9, 44938−44947

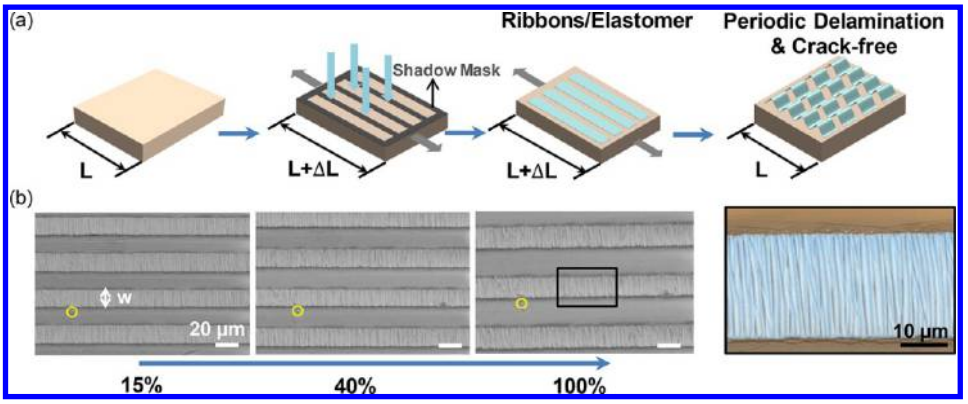


**Figure 3.** Global ordered buckle-delaminated and crack-free pattern in microribbons during their spontaneously buckling-driven delamination on largely prestrained elastomers. (a) Schematic illustration of generating spontaneous buckled delaminated ribbons on prestrained elastomers through shadow mask. (b) SEM images of evolution of buckled delaminated Au ribbons ($t$ = 40 nm, $w$ = 22 $\mu$m) on a 100% prestrained PDMS substrate during the prestrain release, showing no crack formation. Right side shows the magnified view of the buckled delaminated Au ribbons.

process during the prestrain release, we choose a spot as our reference point (RP), noted in Figure 1b, for observation. Figure 1b shows scanning electron microscope (SEM) images of film cracking as a function of the amount of released prestrain. When 15% of the prestrain is released along the horizontal direction, a single crack, parallel to the stretching direction, occurs in the middle. As more prestrain is released, additional parallel cracks appear, and the subsequent cracks approximately divide the fragments at their midpoints to form a nearly ordered cracking pattern. The crack periodicity $d$ in Figure 1b is defined as the average width of unbroken strips, which is measured to be $d = 26.5 \pm 5.1$ $\mu$m after full release of the 100% prestrain. The high-resolution SEM image at the crack location (right of Figure 1b) clearly shows a highly periodic buckled delaminated profile in the stretching direction.

We find that the highly ordered and parallel cracking pattern is present across the whole sample with a large area of 5 mm × 4 mm (Figure S1a). Figure S1b shows that the crack density, defined as the number of cracks per millimeter in the sample, is linearly proportional to the percentage of the prestrain release, which implies that the average cracked fragment width $d$ is inversely proportional to the released prestrain. It should be noted that here the approximately high ordering of cracks is mainly based on the observed cracks largely parallel to the prestrain direction and the absence of longitudinal cracks in the sample. Very recently, the accurate alignment of controlled cracks in terms of both crack positions and distances in metal films deposited on PDMS elastomers has been achieved through the soft island approach proposed by Polywka et al.[36]

**Controllable Spontaneous Periodic Buckle-Delamination.** Similar to periodic wrinkling of thin films on soft substrates without debonding, Figure 2a shows the globally ordered and periodic delaminated patterns in all the gold films on PDMS substrate with different coating thickness and substrate prestrain, demonstrating the ability to control the buckled delaminated patterns. For better control of the periodic buckle-delaminated pattern, quantitative prediction of the delaminated surface topography is needed. Through minimization of the total potential energy in the film−substrate systems, the delamination wavelength $\lambda$, defined as the periodicity of microblisters (inset of Figure 2b), and the amplitude of periodic blisters $A$ can be obtained as

$$\lambda = \pi t\left(\frac{\bar{E}_f t}{\Gamma}\right)^{1/2}\left(\frac{\varepsilon_{pre}}{1+\varepsilon_{pre}}\right)^{1/2}, \quad A = 2t\left(\frac{\bar{E}_f t}{\Gamma}\right)^{1/2}\frac{\varepsilon_{pre}}{(1+\varepsilon_{pre})^{1/2}} \tag{1}$$

where $\bar{E}_f = E_f/(1-\nu_f^2)$ with $E_f$ and $\nu_f$ being the Young's modulus and Poisson's ratio of the film (see Supporting Information). $\Gamma$ is the interfacial toughness between the film and substrate. Figure 2b,c shows the comparison of delamination wavelength $\lambda$ between the theory and experiments for Au film on PDMS substrate as a function of substrate prestrain $\varepsilon_{pre}$ and film thickness $t$. It shows that the theoretical prediction is in good agreement with the experimental results. In eq 1, we assume that Au film has $E_f$ = 61 GPa and $\nu_f$ = 0.35,[37] and $\Gamma$ is equal to the interfacial adhesion energy with $\Gamma \approx 3$ J/m$^2$ set for Au film on PDMS substrate.[38] A difference between the theoretical prediction and experiments is found in Figure 2c for relatively thick Au films. In the theoretical model, both $E_f$ and $\Gamma$ are assumed to remain unchanged for different film thickness. Such a deviation may result from the thickness-dependent material properties of Au films including both Young's modulus and interfacial toughness,[37,38] which will be examined in the future.

**Crack Space Model.** With the assumption that a maximum tensile stress develops at the midpoint between cracked strips, the average width of fragments $d$ can be obtained as[39,40]

$$d = \frac{2t\sigma_c}{E_s(\nu\varepsilon_{pre} - \varepsilon_c)} \tag{2}$$

where $\sigma_c$ and $\varepsilon_c$ are the critical fracture strength and the critical fracture strain of the thin film, respectively (see the Supporting Information for details). $E_s$ and $\nu$ are the Young's modulus and Poisson's ratio of the elastomeric substrate, respectively. Since $\varepsilon_c \ll \varepsilon_{pre}$ for large prestrain over 100%, eq 2 can be approximated as $d \approx 2t\sigma_c/(E_s\nu\varepsilon_{pre})$. Equation 2 shows that, for given materials in the thin film−substrate system, the average width of cracked fragments is inversely proportional to the prestretched strain, while it is linearly proportional to the film thickness. It should be noted that unlike the dependence of buckle-delamination wavelength and amplitude on the interfacial toughness in eq 1, eq 2 shows that the average


DOI: 10.1021/acsami.7b15693
ACS Appl. Mater. Interfaces 2017, 9, 44938−44947

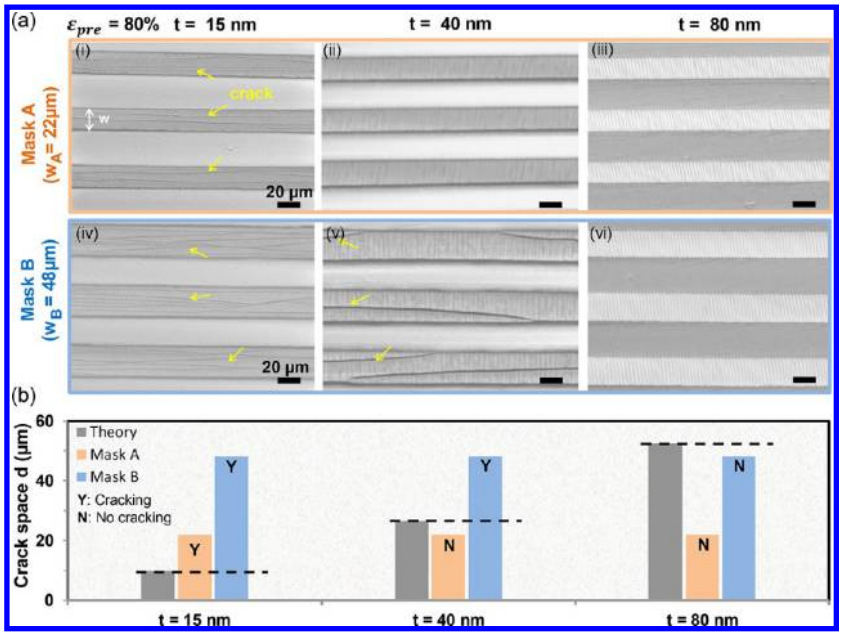


**Figure 4.** Application of the crack space model to the design of crack-free microribbons during their spontaneous buckling delamination on prestrained elastomers. (a) SEM images of the buckled delaminated patterns in Au ribbons with two different ribbon width $w$ values prepared from shadow Mask A ($w_A$ = 22 $\mu$m, top row) and Mask B ($w_B$ = 48 $\mu$m, bottom row) on the same prestrained PDMS substrate with $\varepsilon_{pre}$ = 80%. The thickness of the Au ribbons varies from 15 to 80 nm. (b) Summarization of the competition between the theoretically predicted average crack space $d$ and the ribbon width $w$ in determining the transverse cracking in Au ribbons shown in part a.

width of cracked fragments is independent of the interfacial toughness, implying its negligible role in determining the crack width.

To compare with the simple model in eq 2, we plot the experimental measurements of the average width of cracked fragments, $d$, in both gold (Au) and copper (Cu) thin films on the PDMS substrate ($E_s \approx 2$ MPa, $\nu = 0.49$) as a function of the substrate prestrain $\varepsilon_{pre}$ and coating thickness $t$. Figure 2d shows that, for both Au and Cu films, at $t$ = 40 nm, the increase of $\varepsilon_{pre}$ leads to a monotonic decrease in $d$, which is consistent with the simple model. The fracture strength of Au and Cu thin film can be estimated as 0.25 ± 0.02 and 0.26 ± 0.03 GPa, respectively (Figure S2),[20,21] which also provides the best fit of the simple model (solid curve in Figure 2d) with the experimental results, especially at large prestrain over 100%. When $\varepsilon_{pre}$ = 80% is fixed, Figure 2e shows that for both Au and Cu film, the measured $d$ approximately increases linearly with the film thickness $t$, which mostly agrees with the theoretical prediction. The magnified SEM images in the inset of Figure 2d,e clearly show the highly delaminated profiles of buckled Au and Cu thin film on a PDMS substrate, respectively. The corresponding ordered cracking patterns in the delaminated Au films with different thicknesses are shown in Figure 2a at $\varepsilon_{pre}$ = 80% and 150% (Figure S3). It shows that as $t$ decreases or $\varepsilon_{pre}$ increases, the film cracks into smaller parallel fragments upon full release of the prestrain, showing a higher density of distributed cracks (Figure 2a).

**Design of Crack-Free Spontaneous Periodic Buckle-Delaminated Microribbons in Metal and Silicon.** To eliminate the fragmentation of the film due to Poisson's expansion during release of the prestrain, as illustrated in Figure 3a, we replace the continuous Au thin film with an array of discrete Au ribbons with a fixed ribbon width. Compared to a large-area thin film that cracks, the ribbon pattern provides the ability to control the ribbon width and spacing to avoid cracking, as well as a better control of its electrical performances without cracking. We hypothesize that, for ribbons made of any materials on an elastomer substrate, when the width of ribbons $w$ is set to be equal to or smaller than the average width of cracked fragmentation $d$ in their counterpart of thin film under the identical conditions (i.e., the coating materials and thickness, substrate, and the substrate prestrain are the same), there will be no fragmentation of the spontaneously buckled delaminated ribbons.

As a first step to validate the hypothesis, we fabricated Au ribbons with $w$ = 22 $\mu$m (at the film thickness $t$ = 40 nm), which is smaller than the average crack space $d$ ($d$ = 26.5 ± 5.0 $\mu$m) of its counterpart Au thin film shown in Figure 1b. To deposit the patterned arrays of ribbons, we use a shadow mask by placing it on the top of the prestretched elastomer before the film deposition (see the Experimental Section for more details). Removing the mask leaves the array of deposited ribbons on the stretched substrate. The release of the 100% prestrain in the PDMS leads to the spontaneous delamination of periodic buckled Au ribbons. Figure 3b shows the evolution of buckling in gold ribbons with the increase of released strain. In contrast to the continuous film (Figure 1b), no cracking is observed in the ribbons during and after the full release of the large prestrain (Figure 3b). This is consistent with the hypothesis presented earlier.

Next, we apply the model to design of crack-free buckle-delaminated ribbons with ribbon width $w$ by satisfying $w \leq d$. Figure 4a shows a set of SEM images of spontaneously delaminated Au ribbons with different thickness on a fully released 80% prestrained PDMS substrate. The ribbons are prepared by using two shadow masks with different width: one has a width of $w_A$ = 22 $\mu$m for Mask A (top row of Figure 4a), and the other is $w_B$ = 48 $\mu$m for Mask B (bottom row of Figure 4a). For $t$ = 15, 40, and 80 nm, the corresponding $d$ in Au thin films is predicted to be $d_{15nm}$ = 9.9 $\mu$m, $d_{40nm}$ = 26.7 $\mu$m, and


DOI: 10.1021/acsami.7b15693
ACS Appl. Mater. Interfaces 2017, 9, 44938−44947

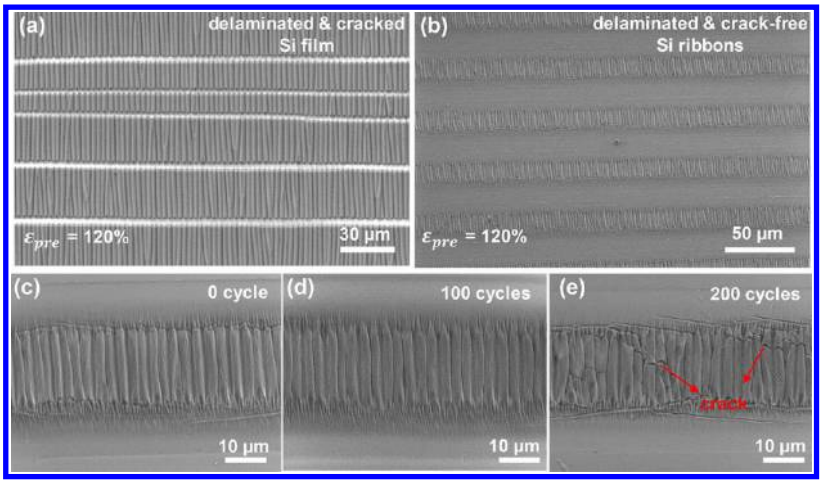


**Figure 5.** Design of crack-free Si ribbons via the crack space model and spontaneous buckling delamination for achieving large stretchability over 100%. SEM images of spontaneously buckled delaminated Si (a) thin films and (b) ribbons ($t$ = 25 nm, $w$ = 22 $\mu$m) on 120% prestrained PDMS substrate. Magnified SEM images of buckled Si ribbons under cycles of mechanical strain releasing and restretching at a strain of 110% after (c) 0, (d) 100, and (e) 200 cycles.

$d_{80nm}$ = 53.4 $\mu$m at $\varepsilon_{pre}$ = 80% in terms of eq 1, respectively. Figure 4b summarizes the comparison between the predicted average width of cracked fragments $d$ and ribbon width $w$ in determining the occurrence of cracking in the buckled delaminated ribbons shown in Figure 4a. It shows that when $w \leq d$, i.e., below the dashed line in Figure 4b in the case of $t$ = 40 nm for Mask A and $t$ = 80 nm for both Mask A and B, no cracks are observed as shown in Figure 4aii,iii,vi, respectively. This agrees well with the hypothesis of no cracking fragmentation when $w \leq d$, with $w_A$ = 22 $\mu$m < $d_{40nm}$ = 26.7 $\mu$m < $w_B$ = 48 $\mu$m < $d_{80nm}$ = 53.4 $\mu$m.

However, above the dashed line in Figure 4b (i.e., $w > d$), cracks are observed in ribbons with $t$ = 15 nm prepared from both masks (Figure 4ai,iv), as well as in ribbons with $t$ = 40 nm for Mask B (Figure 4av). For the case of $t$ = 15 nm, the predicted $d$ in its counterpart thin film is $d_{15nm}$ = 9.9 $\mu$m. For both masks, since $w_B$ = 48 $\mu$m > $w_A$ = 22 $\mu$m > $d_{15nm}$ = 9.9 $\mu$m, in terms of the hypothesis, for $w > d$, cracks will be expected to occur in both cases. Given the same crack density, a larger width of ribbons in Mask B will be expected to have more cracks. These are consistent with the observation in the experiments. For the case of $t$ = 40 nm, $d$ in its counterpart thin film is predicted to be $d_{40nm}$ = 26.7 $\mu$m. For Mask B, we have $d_{40nm}$ = 26.7 $\mu$m < $w$ = $w_B$ = 48 $\mu$m. One or two segmented cracks are observed in most of the ribbons in the experiment (Figure 4av and Figure S4), which is consistent with the hypothesis. In contrast, for ribbons with Mask A, no cracks are observed since $w$ = $w_A$ = 22 $\mu$m < $d_{40nm}$ = 26.7 $\mu$m, which satisfies the hypothesis. Therefore, for design of buckled ribbons without transverse cracking, ribbons should have $w \leq d$.

We assume that the strategy of creating crack-free ribbons by adjusting the pattern of the ribbons could also be applied to less-stretchable materials, e.g., silicon-based materials which are typically more brittle than pure metals. Silicon (Si) in the form of thin films and ribbons through sputtering deposition on 120% prestrained PDMS substrates provides a proof of concept (see the Experimental Section for more details). The evolution of the delaminated pattern in a 25 nm thick Si film with one cycle of substrate prestrain releasing and restretching is shown in Figure S5. It shows that, at a small released strain of 15%, the Si film has already delaminated from the substrate to form periodic but faraway distributed localized buckles. Meanwhile, cracks normal to delaminated buckles are observed. As the released strain further increases, the localized blisters continue to grow and become close to each other to form a globally periodic delaminated buckled pattern, while the cracks become widened. Restretching the sample leads to the close of the cracks as well as the flattening of the periodic delaminated buckles (Figure S5).

The SEM image in Figure 5a shows the periodically delaminated pattern of 25 nm thick deposited Si film with ordered horizontal straight cracks. The measured average width of the cracked fragment is $d$ = 32.4 ± 4.1 $\mu$m. In terms of the validated hypothesis, we choose a smaller width than $d$ in Si ribbon with $w$ = 22 $\mu$m from Mask A, and no cracks are observed in the buckled delaminated Si ribbons (Figure 5b). Figure 5c shows the high-resolution magnified view of the buckled Si ribbons after the first release of the 120% prestrain. Small wrinkles are found in the fringes of the ribbons, i.e., the regions underneath the shadow mask, due to the diffusion of Si during deposition. The mechanical robustness of the buckled delaminated Si ribbons under cyclic mechanical strains is further tested by repeatedly stretching and releasing the samples. Figure 5d,e shows the magnified SEM images of buckled Si ribbons after 100 and 200 cycles of strain releasing and restretching (a strain of 110%). After 100 cycles, no cracks in the ribbons occur (Figure 5d). A few cracks that are aligned with the stretching/releasing direction are observed after 200 cycles (Figure 5e). However, no catastrophic cracking failure is found, demonstrating its repeatability and robustness.

It should be noted that similar constrained buckling-driven periodic delamination in single-crystal silicon ribbons for achieving a large stretchability of about 50% in stretchable electronics was reported by Sun et al.[29] The elastomeric substrate is prepatterned with controlled adhesion sites by applying the lithographically patterned chemistry to the surface; thus, after prestrain release, the ribbons detach from the substrate in the unpatterned nonadhered regions but remain bonded at the designed adhesion spots. Compared to the constrained buckling delamination in their work,[29] the spontaneous and free buckle-delamination in this work could be a complementary and alternative strategy for realizing the large stretchability in stretchable electronics. We showed that controllable periodic buckle-delamination can also be achieved


DOI: 10.1021/acsami.7b15693
ACS Appl. Mater. Interfaces 2017, 9, 44938−44947

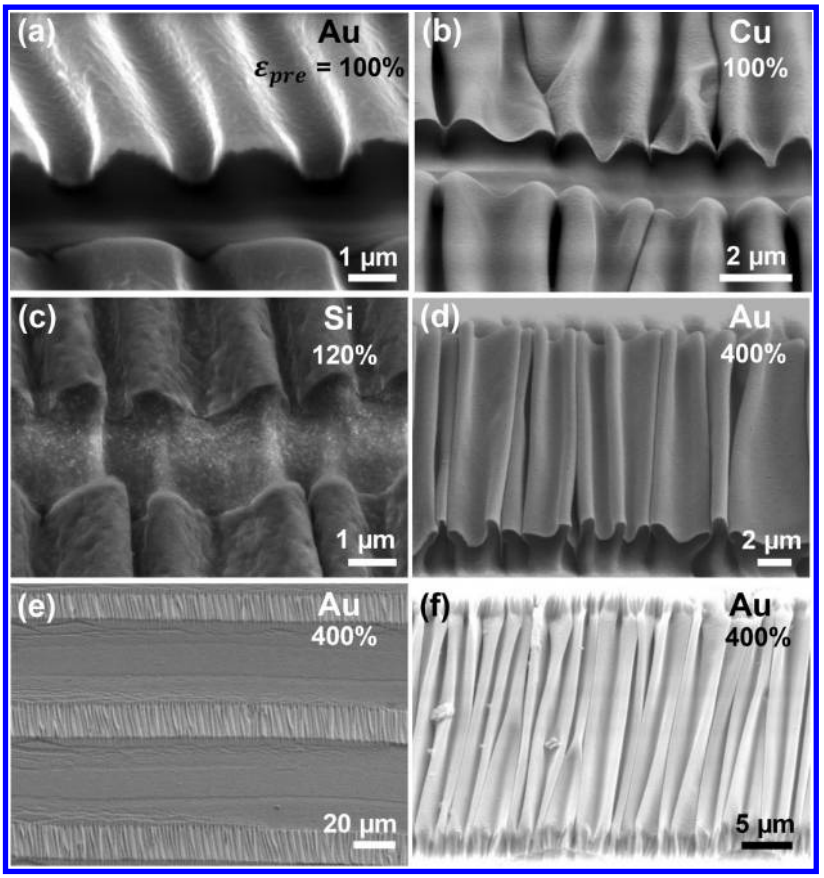


**Figure 6.** Design of crack-free ribbons with guided width for extreme stretchability via spontaneous buckling delamination on prestrained elastomers. High resolution of magnified tilt view of SEM images of buckled delaminated profiles in Au, Cu, and Si thin films on prestrained elastomer substrates at the crack position: (a) Au with $t$ = 25 nm, $\varepsilon_{pre}$ = 100% on PDMS, tilt view angle = 45°; (b) Cu with $t$ = 40 nm, $\varepsilon_{pre}$ = 100% on PDMS, tilt view angle = 30°; (c) Si with $t$ = 25 nm, $\varepsilon_{pre}$ = 120% on PDMS, tilt angle = 0°; (d) Au with $t$ = 40 nm, $\varepsilon_{pre}$ = 400% on silicone rubber, tilt view angle = 45°. (e, f) SEM images of spontaneously buckled delaminated Au ribbon ($t$ = 40 nm, $w$ = 22 $\mu$m) on 400% prestrained silicone rubber. Magnified view is shown in part f.

through spontaneous and free buckling from the substrate without predefined surface adhesion. In addition, despite the absence of potential transverse cracking in the ribbons in Sun et al.'s work,[29] the width of the ribbons is a very important parameter for design of crack-free ribbons to avoid the Poisson's effect induced cracking. The criteria of $w \leq d$ proposed in this work will provide an important theoretical guideline for design of crack-free ribbons for achieving targeted large stretchability.

**Absence of Longitudinal Cracks in Spontaneous Periodic Buckle-Delamination.** In addition to the periodic transverse cracks that are aligned with the direction of prestrain because of the Poisson effect discussed so far, it is possible for longitudinal cracks orthogonal to the prestrain direction to occur in both buckled delaminated films and ribbons. Normally, the peaks of the delaminated buckles are under severe tension and experience the maximum tensile strain in the film. When the maximum tensile strain, i.e., peak strain, is beyond the onset of fracture strain of the coated materials, longitudinal cracking will occur, initiating from the wave crests and propagating along the blisters. Interestingly, despite the existence of cracking fragmentation in the thin films or ribbons, no longitudinal cracks along the blisters are observed throughout all the delaminated buckled Au (Figures 1b, 2a, 3b, and 4, and Figure S3), Cu (Figure 2e), and Si (Figure 5) thin films or ribbons on over 100% prestrained PDMS studied so far. Specially, for buckled silicon ribbons on 120% prestrained PDMS, after 200 cycles, there are still no longitudinal cracks observed (Figure 5e), which could enable a potential high stretchability by harnessing spontaneous buckling-driven delamination.

To better understand the absence of longitudinal cracks in the spontaneously buckled delaminated patterns, we examine the maximum tensile strain in different coatings. Figure 6a–c shows the high-resolution cross sections of delaminated buckles in Au, Cu, and Si thin film at $\varepsilon_{pre} \geq$ 100%. The maximum tensile strain in the thin film can be approximately given by the maximum bending strain of $\varepsilon_{max} = \kappa_{max} t/2$ with $\kappa_{max}$ being the maximum bending curvature. The measurements of the curvatures imply that the maximum tensile strain in the Au and Cu film is ~1.3% and ~2.5% for a large 100% prestrain, respectively. Specially, for Si film, $\varepsilon_{max}$ is ~1.1%, which is below its fracture strain of ~2% and ~100 times smaller than its substrate prestrain of 120%. The small strain in the thin films for over 100% substrate prestrain is due to the large strain relaxation through spontaneously buckling-driven delamination, and thus enables potential high stretchability.

**Extreme Stretchability via Spontaneous Periodic Buckled Delamination.** To demonstrate the potential for spontaneous buckled delamination to achieve extreme stretchability, we increase the substrate prestrain from 100% to 400% by replacing PDMS with a more stretchable silicone rubber substrate. Figure S6 shows the transversely fragmented and


DOI: 10.1021/acsami.7b15693
ACS Appl. Mater. Interfaces 2017, 9, 44938–44947

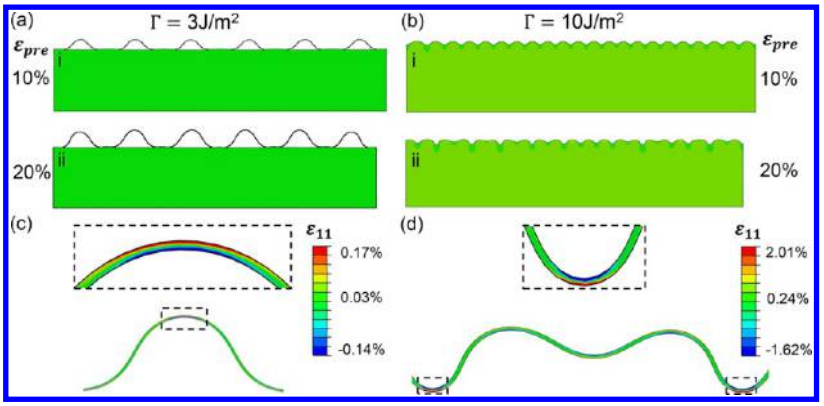


**Figure 7.** FEM simulation results on the effect of interfacial toughness Γ on buckling of Au coatings on prestrained PDMS substrate. (a) Spontaneous periodic buckle-delamination at Γ = 3 J/m$^2$ after release of 10% and 20% prestrain. (b) Wrinkling to period-doubling transition at Γ = 10 J/m$^2$ after release of 10% and 20% prestrain. (c, d) Corresponding strain contour in the buckle-delamination and period-doubling wrinkles after 20% prestrain release.

buckled delaminated Au films ($t$ = 40 nm) on a 400% prestrained silicone rubber substrate. No longitudinal cracks along the buckles are observed in the delaminated Au film. The magnified view of the SEM image in Figure 6d shows that the extremely buckled profiles exhibit a complex combination of deep creases, period doubling buckling delamination, and jigsaw-like shapes. The bottoms of the deep creases are adhered to the elastomer substrate and define the support points for the highly delaminated film. The maximum tensile strain in the Au film is ∼3.2% from the measurement of curvatures, over 100 times smaller than the substrate prestrain of 400% and below the fracture strain of 5% of Au.[41] It should be noted that, despite the absence of cracks, the high tensile strain may cause localized yielding of the film. For a delay of the potential yielding at large strain, lowering the maximum tensile strain is possible by further reducing its thickness, which will be explored in the future work.

The absence of longitudinal cracks in the Au film at an extremely large 400% prestrain enables the design of crack-free Au ribbons for achieving potential extreme stretchability. Guided by our validated hypothesis, for a Au ribbon ($t$ = 40 nm), for the acquisition of stretchability of 400% without inducing transverse cracking, i.e., a substrate prestrain of 400%, the designed width of the ribbon $w$ should satisfy $w \leq d = 22.4$ $\mu$m predicted by eq 2 (here $E_s$ = 0.45 MPa and $\nu$ = 0.49 for silicone rubber substrate). Thus, we choose $w$ = 22 $\mu$m for the Au ribbon width for proof of concept. Figure 6e shows the spontaneous buckled delaminated pattern in the designed ribbons with $w$ = 22 $\mu$m after full release of 400% substrate prestrain, which exhibits no transverse cracks in the ribbons. The magnified view of the SEM image in Figure 6f also shows that no longitudinal cracks along the buckles are observed. Thus, the absence of cracks in both directions in Au ribbons validates our design of crack-free ribbons for achieving potential extreme stretchability via spontaneously buckling-driven delamination.

**Spontaneous Periodic Buckle-Delamination versus Spontaneous Wrinkling in Strain Release.** To better understand the advantage of spontaneous periodic buckle-delamination over wrinkling in releasing the strain in the coating, we conducted finite element method (FEM) simulations to reveal the quantitative information on the maximum strain level in the coatings by manipulating the interfacial toughness between the coating and the substrate (see the Experimental Section for more details).

Figure 7 shows the simulation results on the comparison of the same Au coating on prestrained PDMS substrates with two different interfacial toughness Γ values. It shows that when Γ = 3 J/m$^2$, after strain release of 10%, periodic buckle-delaminated blisters are formed (Figure 7ai). Further relatively larger strain release of 20% leads to the growth of both amplitude and width of the blisters (Figure 7aii). This is consistent with both experiments and theoretical model. In contrast, when Γ increases from 3 to 10 J/m$^2$, periodic sinusoidal wrinkles are formed with both much smaller amplitude and wavelength after 10% strain release (Figure 7bi). Further release of 20% results in the transition from sinusoidal to period-doubling wrinkles[42,43] (Figure 7bii). The simulated strain contours in both cases after 20% prestrain release are shown in Figure 7c,d. It shows that the maximum tensile strain in the coating via buckle-delamination is around 0.17% located at the wave crest, which is over 100 times smaller than the prestrain. In contrast, the maximum tensile strain in the coating via period-doubling wrinkles is located at the wave troughs of smaller wrinkles and is over 10 times larger than that via buckle-delamination, proving that spontaneous periodic buckle-delamination is a more effective way to release the accumulated strain in the same coating as compared to wrinkling.

**Application to Design of Stretchable Electronics via Spontaneous Buckle-Delamination of Au Ribbons.** Next, we apply the principle of crack-free and spontaneous periodic buckle-delamination to the design of Au ribbons for stretchable electronics as a proof-of-concept demonstration. It should be noted that normally both transverse and longitudinal cracks in ribbons should be avoided in design of stretchable electronics. The presence of cracks will not only break the integrity and mechanical robustness of the whole structure but also degrade its electrical performance in terms of high electrical resistance. For a targeted stretchability of 200% in Au ribbons with Au thickness of 80 nm on silicone rubber substrate, the ribbon width is set to be 60 $\mu$m to avoid the cracks, which is less than the predicted critical crack fragmentation width of 88 $\mu$m. After full release of the 200% substrate prestrain, it does show the absence of cracks in the spontaneously and periodic buckle-delaminated Au ribbons (inset of Figure 8a). The electrical resistance of the crack-free buckle-delaminated Au ribbons $R_0$ is measured to be around 24 Ω by following the setup as


DOI: 10.1021/acsami.7b15693
ACS Appl. Mater. Interfaces 2017, 9, 44938−44947

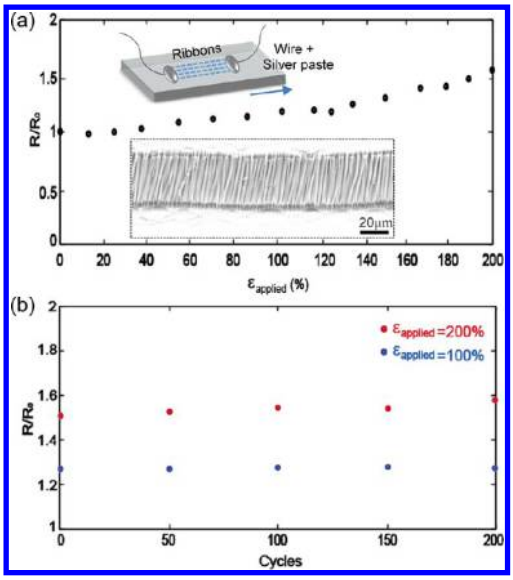


**Figure 8.** Measurement of normalized electrical resistance for Au ribbons on silicone rubber substrates under mechanical deformation. (a) Normalized resistance of buckle-delaminated Au ribbons ($t$ = 80 nm and $w$ = 60 $\mu$m) as a function of applied strain. Insets are the schematic illustration of experimental setup (top) and SEM image of Au ribbons at initial buckle-delaminated state ($R/R_0$ = 1). (b) Mechanical cycling results of normalized resistance at different applied strains 100% and 200%.

schematically illustrated in the inset of Figure 8a. Then, we restretch the buckle-delaminated Au ribbons to evaluate their resistance change $R/R_0$ as a function of the applied strain $\varepsilon_{applied}$. Figure 8a shows that, for $\varepsilon_{applied} \leq 120\%$, the electrical resistance $R$ increases slightly by 10%, and the increase of the applied strain has a slight effect on its resistance. When $\varepsilon_{applied}$ is further increased, $R/R_0$ increases gradually. As $\varepsilon_{applied}$ = 200%, the initial buckle-delaminated ribbons are fully stretched and become flattened; correspondingly, it leads to a 60% increase in its resistance when compared to the original buckled state due to the loss of contacts between neighboring delaminated buckles. For highly buckle-delaminated ribbons after strain release, the periodic delaminated buckles become contacted with their neighboring ones; thus, the connection between contacted blisters results in a reduced electrical conductor length when compared to the flat state under fully stretched state. Since the electrical resistance is proportional to the length of the conductor $l$, the reduced $l$ in the periodic buckle-delamination leads to a lower electrical resistance as compared to that of flattened ribbons without neighboring contacts after being fully stretched. It should be noted that the moderate increase in resistance also implies that the restretching process generates no cracks in the ribbons since the presence of cracks will lead to a significant increase of the electrical resistance, which is validated by the observation of free cracks. The mechanical robustness of its stable electrical property is verified under cyclic strain release and restretching. Figure 8b shows the normalized electrical resistance $R/R_0$ as a function of the number of cycles under an applied strain of 100% and 200%. It shows that the resistance remains nearly unchanged after 200 cycles. In our longest tests, the electrical resistance remains stable after 1000 cycles, indicating that no cracking failure occurs in the samples.

## CONCLUSION

In conclusion, we demonstrated design of highly stretchable crack-free microribbons by exploiting spontaneous buckling-driven delamination in both metal and silicon materials. The transverse cracking fragmentation due to the Poisson effect in the buckled microribbons can be avoided by setting the width of the ribbon to be equal to or smaller than the average width of cracked fragments in their counterpart thin films. The longitudinal cracks along the buckles are largely suppressed via spontaneous buckled delamination to release the strain more efficiently. The maximum tensile strain in the delaminated microribbons, which is about 100 times smaller than the substrate prestrain, enables the potential extreme stretchability. The strategies presented here could have potential applications in design of stretchable electronics, stretchable energy storage devices, crack control in thin films, and self-assembly of 3D microstructures.[44]

## ASSOCIATED CONTENT

### Supporting Information

The Supporting Information is available free of charge on the ACS Publications website at DOI: 10.1021/acsami.7b15693.

SEM images, crack density vs released strain, fracture strength vs prestrain, AFM profiles, and calculation details (PDF)

## AUTHOR INFORMATION

### Corresponding Author

*E-mail: jieyin@temple.edu.

### ORCID

Kevin T. Turner: 0000-0003-4963-4568

Jie Yin: 0000-0002-6297-1262

### Notes

The authors declare no competing financial interest.

## ACKNOWLEDGMENTS

J.Y. acknowledges the funding support from the start-up at Temple University and National Science Foundation (NSF) (CMMI-1727792).

## REFERENCES

(1) Genzer, J.; Groenewold, J. Soft Matter with Hard Skin: From Skin Wrinkles to Templating and Material Characterization. *Soft Matter* **2006**, *2*, 310−323.

(2) Yang, S.; Khare, K.; Lin, P.-C. Harnessing Surface Wrinkle Patterns in Soft Matter. *Adv. Funct. Mater.* **2010**, *20*, 2550−2564.

(3) Chen, X.; Yin, J. Buckling Patterns of Thin Films on Curved Compliant Substrates with Applications to Morphogenesis and Three-Dimensional Micro-Fabrication. *Soft Matter* **2010**, *6*, 5667−5680.

(4) Mei, Y.; Kiravittaya, S.; Harazim, S.; Schmidt, O. G. Principles and Applications of Micro and Nanoscale Wrinkles. *Mater. Sci. Eng., R* **2010**, *70*, 209−224.

(5) Singamaneni, S.; Tsukruk, V. V. Buckling Instabilities in Periodic Composite Polymeric Materials. *Soft Matter* **2010**, *6*, 5681−5692.

(6) Chung, J. Y.; Nolte, A. J.; Stafford, C. M. Surface Wrinkling: A Versatile Platform for Measuring Thin-Film Properties. *Adv. Mater.* **2011**, *23*, 349−368.

(7) Li, B.; Cao, Y.-P.; Feng, X.-Q.; Gao, H. Mechanics of Morphological Instabilities and Surface Wrinkling in Soft Materials: A Review. *Soft Matter* **2012**, *8*, 5728−5745.

(8) Wang, Q.; Zhao, X. Beyond Wrinkles: Multimodal Surface Instabilities for Multifunctional Patterning. *MRS Bull.* **2016**, *41*, 115−122.



DOI: 10.1021/acsami.7b15693
*ACS Appl. Mater. Interfaces* 2017, 9, 44938−44947

(9) Lin, G.; Chandrasekaran, P.; Lv, C.; Zhang, Q.; Tang, Y.; Han, L.; Yin, J. Self-Similar Hierarchical Wrinkles as a Potential Multifunctional Smart Window with Simultaneously Tunable Transparency, Structural Color, and Droplet Transport. *ACS Appl. Mater. Interfaces* **2017**, *9*, 26510−26517.
(10) Lin, G.; Ge, D.; Tang, Y.; Xia, Y.; Wu, G.; Han, L.; Yang, S.; Yin, J. Cuts Guided Deterministic Buckling in Arrays of Soft Parallel Plates for Multifunctionality. *ACS Appl. Mater. Interfaces* **2017**, *9*, 29345−29354.
(11) Saif, M. T. A. On a Tunable Bistable Mems-Theory and Experiment. *J. Microelectromech. Syst.* **2000**, *9*, 157−170.
(12) Qiu, J.; Lang, J. H.; Slocum, A. H. A Centrally-Clamped Parallel-Beam Bistable Mems Mechanism. *Technical Digest MEMS 2001 14th IEEE International Conference on Micro Electro Mechanical Systems* **2001**, 353−356.
(13) Rogers, J. A.; Someya, T.; Huang, Y. Materials and Mechanics for Stretchable Electronics. *Science* **2010**, *327*, 1603−1607.
(14) Park, S.; Vosguerichian, M.; Bao, Z. A Review of Fabrication and Applications of Carbon Nanotube Film-Based Flexible Electronics. *Nanoscale* **2013**, *5*, 1727−1752.
(15) Sekitani, T.; Someya, T. Stretchable, Large-Area Organic Electronics. *Adv. Mater.* **2010**, *22*, 2228−2246.
(16) Yao, S.; Zhu, Y. Nanomaterial-Enabled Stretchable Conductors: Strategies, Materials and Devices. *Adv. Mater.* **2015**, *27*, 1480−1511.
(17) Xu, S.; Yan, Z.; Jang, K.-I.; Huang, W.; Fu, H.; Kim, J.; Wei, Z.; Flavin, M.; McCracken, J.; Wang, R.; Badea, A.; Liu, Y.; Xiao, D.; Zhou, G.; Lee, J.; Chung, H. U.; Cheng, H.; Ren, W.; Banks, A.; Li, X.; Paik, U.; Nuzzo, R. G.; Huang, Y.; Zhang, Y.; Rogers, J. A. Assembly of Micro/Nanomaterials into Complex, Three-Dimensional Architectures by Compressive Buckling. *Science* **2015**, *347*, 154−159.
(18) Zhang, Y.; Yan, Z.; Nan, K.; Xiao, D.; Liu, Y.; Luan, H.; Fu, H.; Wang, X.; Yang, Q.; Wang, J.; Ren, W.; Si, H.; Liu, F.; Yang, L.; Li, H.; Wang, J.; Guo, X.; Luo, H.; Wang, L.; Huang, Y.; Rogers, J. A. A Mechanically Driven Form of Kirigami as a Route to 3d Mesostructures in Micro/Nanomembranes. *Proc. Natl. Acad. Sci. U. S. A.* **2015**, *112*, 11757−11764.
(19) Zang, J.; Ryu, S.; Pugno, N.; Wang, Q.; Tu, Q.; Buehler, M. J.; Zhao, X. Multifunctionality and Control of the Crumpling and Unfolding of Large-Area Graphene. *Nat. Mater.* **2013**, *12*, 321−325.
(20) Thomas, A. V.; Andow, B. C.; Suresh, S.; Eksik, O.; Yin, J.; Dyson, A. H.; Koratkar, N. Controlled Crumpling of Graphene Oxide Films for Tunable Optical Transmittance. *Adv. Mater.* **2015**, *27*, 3256−3265.
(21) Hutchinson, J. W.; Thouless, M. D.; Liniger, E. G. Growth and Configurational Stability of Circular, Buckling-Driven Film Delaminations. *Acta Metall. Mater.* **1992**, *40*, 295−308.
(22) Ortiz, M.; Gioia, G. The Morphology and Folding Patterns of Buckling-Driven Thin-Film Blisters. *J. Mech. Phys. Solids* **1994**, *42*, 531−559.
(23) Jensen, H. M.; Sheinman, I. Straight-Sided, Buckling-Driven Delamination of Thin Films at High Stress Levels. *Int. J. Fract.* **2001**, *110*, 371−385.
(24) Moon, M. W.; Jensen, H. M.; Hutchinson, J. W.; Oh, K. H.; Evans, A. G. The Characterization of Telephone Cord Buckling of Compressed Thin Films on Substrates. *J. Mech. Phys. Solids* **2002**, *50*, 2355−2377.
(25) Mei, H.; Huang, R.; Chung, J. Y.; Stafford, C. M.; Yu, H.-H. Buckling Modes of Elastic Thin Films on Elastic Substrates. *Appl. Phys. Lett.* **2007**, *90*, 151902.
(26) Mei, H.; Landis, C. M.; Huang, R. Concomitant Wrinkling and Buckle-Delamination of Elastic Thin Films on Compliant Substrates. *Mech. Mater.* **2011**, *43*, 627−642.
(27) Pan, K.; Ni, Y.; He, L.; Huang, R. Nonlinear Analysis of Compressed Elastic Thin Films on Elastic Substrates: From Wrinkling to Buckle-Delamination. *Int. J. Solids Struct.* **2014**, *51*, 3715−3726.
(28) Vella, D.; Bico, J.; Boudaoud, A.; Roman, B.; Reis, P. M. The Macroscopic Delamination of Thin Films from Elastic Substrates. *Proc. Natl. Acad. Sci. U. S. A.* **2009**, *106*, 10901−10906.
(29) Sun, Y.; Choi, W. M.; Jiang, H.; Huang, Y. Y.; Rogers, J. A. Controlled Buckling of Semiconductor Nanoribbons for Stretchable Electronics. *Nat. Nanotechnol.* **2006**, *1*, 201−207.
(30) Khang, D.-Y.; Jiang, H.; Huang, Y.; Rogers, J. A. A Stretchable Form of Single-Crystal Silicon for High-Performance Electronics on Rubber Substrates. *Science* **2006**, *311*, 208−212.
(31) Efimenko, K.; Rackaitis, M.; Manias, E.; Vaziri, A.; Mahadevan, L.; Genzer, J. Nested Self-Similar Wrinkling Patterns in Skins. *Nat. Mater.* **2005**, *4*, 293−297.
(32) Xuan, Y.; Guo, X.; Cui, Y.; Yuan, C.; Ge, H.; Cui, B.; Chen, Y. Crack-Free Controlled Wrinkling of a Bilayer Film with a Gradient Interface. *Soft Matter* **2012**, *8*, 9603−9609.
(33) Carlson, A.; Bowen, A. M.; Huang, Y.; Nuzzo, R. G.; Rogers, J. A. Transfer Printing Techniques for Materials Assembly and Micro/Nanodevice Fabrication. *Adv. Mater.* **2012**, *24*, 5284−5318.
(34) Gou, H.-L.; Xu, J.-J.; Xia, X.-H.; Chen, H.-Y. Air Plasma Assisting Microcontact Deprinting and Printing for Gold Thin Film and Pdms Patterns. *ACS Appl. Mater. Interfaces* **2010**, *2*, 1324−1330.
(35) Yu, S.; Sun, Y.; Ni, Y.; Zhang, X.; Zhou, H. Controlled Formation of Surface Patterns in Metal Films Deposited on Elasticity-Gradient Pdms Substrates. *ACS Appl. Mater. Interfaces* **2016**, *8*, 5706−5714.
(36) Polywka, A.; Stegers, L.; Krauledat, O.; Riedl, T.; Jakob, T.; Görrn, P. Controlled Mechanical Cracking of Metal Films Deposited on Polydimethylsiloxane (Pdms). *Nanomaterials* **2016**, *6*, 168.
(37) Akogwu, O.; Kwabi, D.; Midturi, S.; Eleruja, M.; Babatope, B.; Soboyejo, W. O. Large Strain Deformation and Cracking of Nano-Scale Gold Films on Pdms Substrate. *Mater. Sci. Eng., B* **2010**, *170*, 32−40.
(38) Oyewole, O. K.; Yu, D.; Du, J.; Asare, J.; Oyewole, D. O.; Anye, V. C.; Fashina, A.; Kana, M. G. Z.; Soboyejo, W. O. Micro-Wrinkling and Delamination-Induced Buckling of Stretchable Electronic Structures. *J. Appl. Phys.* **2015**, *117*, 235501.
(39) Volynskii, A. L.; Bazhenov, S.; Lebedeva, O. V.; Ozerin, A. N.; Bakeev, N. F. Multiple Cracking of Rigid Platinum Film Covering Polymer Substrate. *J. Appl. Polym. Sci.* **1999**, *72*, 1267−1275.
(40) Bazhenov, S. L.; Volynskii, A. L.; Alexandrov, V. M.; Bakeev, N. F. Two Mechanisms of the Fragmentation of Thin Coatings on Rubber Substrates. *J. Polym. Sci., Part B: Polym. Phys.* **2002**, *40*, 10−18.
(41) Fan, J. A.; Yeo, W.-H.; Su, Y.; Hattori, Y.; Lee, W.; Jung, S.-Y.; Zhang, Y.; Liu, Z.; Cheng, H.; Falgout, L.; Bajema, M.; Coleman, T.; Gregoire, D.; Larsen, R. J.; Huang, Y.; Rogers, J. A. Fractal Design Concepts for Stretchable Electronics. *Nat. Commun.* **2014**, *5*, 3266.
(42) Brau, F.; Vandeparre, H.; Sabbah, A.; Poulard, C.; Boudaoud, A.; Damman, P. Multiple-Length-Scale Elastic Instability Mimics Parametric Resonance of Nonlinear Oscillators. *Nat. Phys.* **2011**, *7*, 56−60.
(43) Cao, Y.; Hutchinson, J. W. Wrinkling Phenomena in Neo-Hookean Film/Substrate Bilayers. *J. Appl. Mech.* **2012**, *79*, 031019−031019−9.
(44) Cavallo, F.; Turner, K. T.; Lagally, M. G. Facile Fabrication of Ordered Crystalline-Semiconductor Microstructures on Compliant Substrates. *Adv. Funct. Mater.* **2014**, *24*, 1730−1737.


DOI: 10.1021/acsami.7b15693
*ACS Appl. Mater. Interfaces* 2017, 9, 44938−44947